Biophysical Chemistry 202 (2015) 1–12

Contents lists available at ScienceDirect

Biophysical Chemistry

journal homepage: http://www.elsevier.com/locate/biophyschem

Structural insight into the mechanism of amyloid precursor protein recognition by β-secretase 1: A molecular dynamics study

Sandipan Chakraborty *, Soumalee Basu **

Department of Microbiology, University of Calcutta, 35 Ballygunge Circular Road, Kolkata 700 019, India

HIGHLIGHTS

- Free BACE1 exists as a conformational ensemble, visits both open and closed forms.
- Concerted movement of flap and other loops leads to open to closed transition.
- Cavity closing of BACE1 is a hinge movement between the N- and C-terminal domains.
- Binding of APP to the BACE1 is a conformational selection process.
- Flap region appropriately orients the APP cut-site towards the catalytic ASP dyad.

GRAPHICAL ABSTRACT

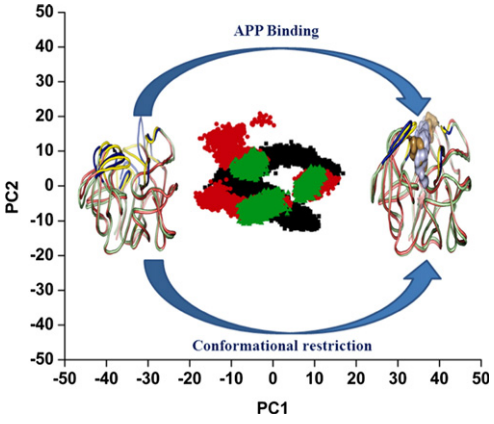

Free BACE1 is highly flexible and exists as an ensemble of conformations. The β-hairpin flap and other loop regions of the active site of BACE1 visit numerous conformations during the simulation. During the simulation time-scale, BACE1 visits both the open and closed form multiple times. Binding of APP to the BACE1 cavity shifts the equilibrium towards a stable complex.

ARTICLE INFO

Article history:
Received 13 January 2015
Received in revised form 8 March 2015
Accepted 9 March 2015
Available online 25 March 2015

Keywords:
BACE1
APP
Molecular dynamics simulation
Essential dynamics
Conformational switching
Electrostatic surface complementarity

ABSTRACT

β-secretase 1 (BACE1) initiates the proteolysis of amyloid precursor protein (APP) to generate Aβ, aggregation of which has been considered to be the main histopathological feature of Alzheimer's Disease. Here, we have explored the conformational switching of BACE1 during APP recognition using molecular dynamics simulation thereby suggesting the recognition to be a conformational selection process. Free BACE1 is highly flexible and exists as an ensemble of conformations. The β-hairpin flap that covers the active site of BACE1 visits numerous conformations during the simulation. Essential dynamics reveal that concerted movements in several loops including the flap region lead to a conformational switching from open to closed form. During the simulation, free BACE1 visits both the open and closed forms multiple times. Binding of APP to the BACE1 cavity shifts the equilibrium towards a stable complex stabilized by strong electrostatic surface complementarity along with several van der Waals and hydrogen bonding interactions.

* Corresponding author.
** Corresponding author. Tel.: +91 33 4615445/4711/4712.Extn.341/342; fax: +91 33 24614849.
E-mail addresses: sandipanchakraborty.13@gmail.com (S. Chakraborty), soumalee@gmail.com (S. Basu).

http://dx.doi.org/10.1016/j.bpc.2015.03.006
0301-4622/

1. Introduction

Alzheimer's Disease (AD) is the most frequently observed neurodegenerative disorder characterized by progressive dementia with declining cognitive behavior [1,2]. Presence of neuritic plaques composed of aggregated amyloid β peptide (Aβ) in the hippocampus, cerebral cortex and entorhinal cortex has been considered to be the main pathological feature of AD [3,4]. Aβ is generated due to aberrant proteolysis of a membrane protein, the amyloid precursor protein (APP) [5]. β-Secretase 1 (BACE1) initially cleaves APP at the N-terminus of the amyloid beta (Aβ) peptide domain which is followed by the second cleavage within the transmembrane domain of APP by γ-secretase [6,7]. Schematic representation of APP proteolysis is summarized in Scheme 1A. BACE1 is an aspartate protease, catalyzing the first step of Aβ peptide generation and also BACE1 knock-out mice lacking Aβ production exhibits normal physiology [8]. These observations make BACE1 a prime target to design therapeutics in AD.

At present, there is a remarkable growth in research interest to study the structure of BACE1 in the APO form and in complex with designed or synthesized inhibitors [9–14]. Comparison of several BACE1 crystal structures and molecular modeling studies of BACE1–inhibitor complexes reveal that the protein possesses a high degree of conformational flexibility [9–11,15]. The catalytic cavity of the protein undergoes significant structural changes upon ligand binding [9,15], giving rise to open and closed forms [9,10,15]. Particularly, the β-hairpin "Flap region" (residue 67–77), which covers the opening of the catalytic cavity of BACE1, can adopt different conformations in the open and the closed form [9]. In the presence of bound peptides or peptide-like inhibitors [11,12,16], the flap moves closer to the catalytic aspartate dyad to tightly retain the inhibitors within the active site, representing the "closed conformation" of BACE1. Comparison of several inhibitor bound BACE1 structures reveals variety of flap conformations whose position and orientation depend on the volume of the bound inhibitors. Recently, Xu et al. [17] reported two crystal structures of BACE1 bound to the same inhibitor belonging to two different space groups, exhibiting different flap orientations. They further carried out systematic analysis of all the BACE1–inhibitor complexes available in the PDB database which revealed that hydrogen-bonding interactions between main-chain atoms of the flap residues and the bound inhibitor lock the flap in the closed conformation [17], while in other complexes where the flap adopts a relatively open conformation, the inhibitors resist flap closing [17] due to steric clashes. An interesting observation is that most of the crystal structures of the BACE1–inhibitor complexes belonging to space group P6122, exhibit open flap conformation [17]. Thus there is a strong influence of crystal packing on the flap orientation of BACE1–inhibitor complexes. In the APO structures, the flap is generally observed to adopt an open conformation [18,19]. But again, the orientation and exposure of flap opening greatly varies in different reported crystal structures. Moreover, MD simulations revealed that in the absence of the peptidic inhibitor, OM99-2, the flap can switch between the open and the closed form, within a timescale of 10 ns [15]. Even a self-inhibitory conformation of TYR 71 has also been observed [18] in the unbound crystal of the enzyme. Recently, by using elastic network model, we have demonstrated that significant flexibility in other loop regions of the active site such as "10s loop" (residues 9–14) located between two strands at the base of the S3 subpocket, "A loop" (residues 158–167), "F loop" (residues 311–318) and the "D loop" (residues 270–273) is crucial for inhibitor recognition [10]. Thus BACE1 exhibits significant ligand induced conformational flexibility in its active site. An overview of the different loop regions that line the active site cavity of BACE1 is shown in Scheme 1B.

It has also been reported that BACE1 activity is optimal at an acidic pH which has been attributed to the particular protonation state of the catalytic aspartate dyad [15,19]. Interestingly, BACE1 and APP follow similar cellular trafficking pathways [20]. At the plasma membrane, they are mainly co-localized in lipid rafts where the pH being ~7 [21], BACE1 shows poor catalytic activity. From there, both BACE1 and APP are compartmentalized within endosomes by trafficking through

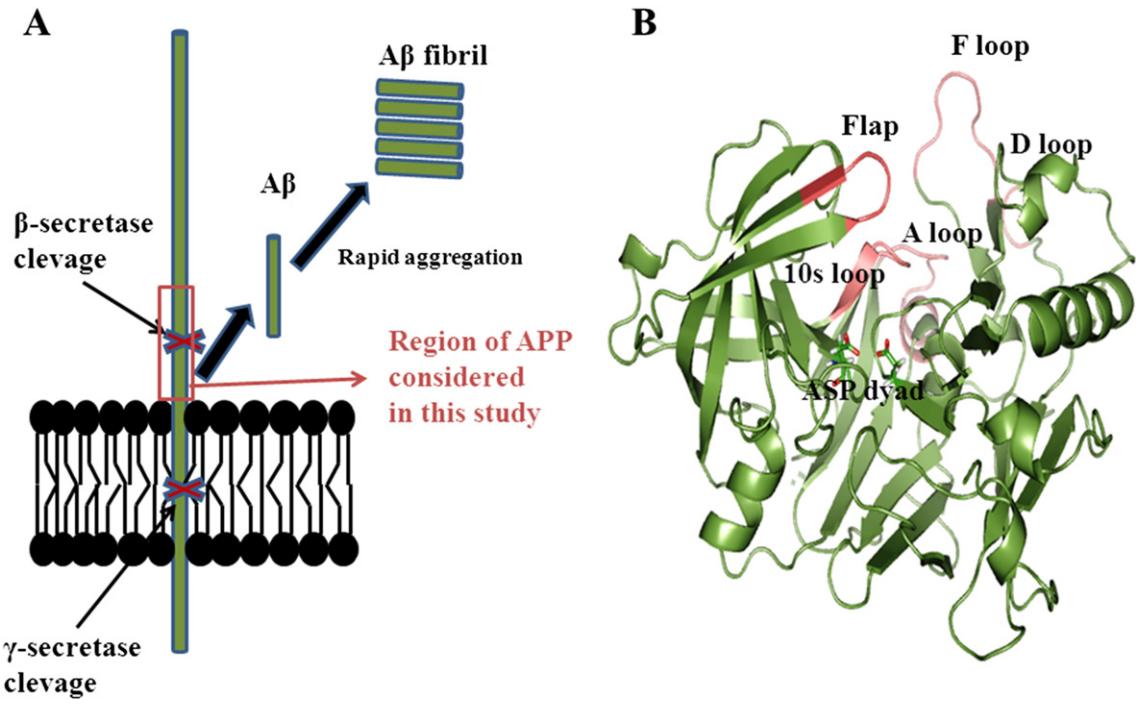

Scheme 1. A: Schematic representation of the amyloid precursor protein (APP) processing and amyloid fibril formation observed in Alzheimer's Disease. In amyloidogenic pathway, successive cleavage by β-site APP-cleaving enzyme (BACE1) followed by γ-secretase releases the highly aggregate prone peptide, Aβ, which rapidly aggregates in a nucleation-dependent manner to form "Amyloid fibril" that has the characteristic β-sheeted arrangement. Region of APP around the β-cleavage site considered in this study to probe BACE1–APP interaction is shown within the box. B: Cartoon representation of BACE1. Different loopy regions that frames the active site cavity of BACE1, flap residues (67–77), 10s loop, F loop colored in red. Catalytic aspartate dyad is rendered in stick representation.

trans-Golgi network [22,23], where BACE1 is activated due to an acidic environment (pH 4.5 to 6). Considering the long half-life of BACE1, it is assumed that these cellular sorting pathways are repeated many times throughout the lifespan of the enzyme. Recent live-cell imaging and selective labeling of BACE1 in hippocampal neurons suggest that the transport vesicles containing internalized BACE1 in dendrites undergo retrograde transport towards the soma, whereas they undergo bidirectional transport in axons [24]. Recently, Shimizu et al. determined the crystal structure of the active form of BACE1 and they predicted that during substrate binding there is a conformational switching which activates the protein at low pH [19]. Also, particular orientation of the aspartate dyad and conserved hydrogen bonding interaction network is highly crucial for the proteolysis of APP [15,19]. These observations implicate that the catalytic properties of BACE1 are modulated by large-scale conformational changes between the active and inactive forms [19]. Interconvertibility between the active and the inactive states of BACE1 under physiological conditions plays an important role in the localization-dependent activity of BACE1 [19].

However, the structural details of the conformational switching during APP recognition are not known, even the crystal structure of active BACE1 in the presence of bound APP is yet to be solved. In a preliminary study, Sauder et al. [25] modeled BACE1 in complex with a six residue APP fragment using homology modeling, but did not take into account the conformational changes induced by APP for such a flexible protein like BACE1. Currently two most probable hypotheses of substrate recognition are accepted [26,27], one is conformational selection and the other is induced fit. In the conformational selection approach, the ligand selectively binds to a receptor conformation among preexisting ensemble of conformations, where it finds suitable complementarity with the receptor and ligand recognition leads to an equilibrium shift towards the most stable protein–ligand complex. Induced fit approximation is generally associated with substrate induced structural changes in the receptor. We, for the first time present a detailed mechanism of APP recognition by BACE1 and also study the conformational switching that occurs upon APP binding to the active site cleft of BACE1 by using extensive molecular dynamics simulations. We have also explored the necessary interaction required for BACE1 to recognize APP by using several in silico techniques.

2. Materials and methods

2.1. Modeling of APP and BACE1

In this study, we considered a 30 residue APP fragment which contains the known APP cut-site. The 30 residue APP fragment was modeled as helix in such a way that the cut-site was in the middle. Since, during binding to BACE1, APP is embedded within the membrane, we modeled the APP fragment as helical. The initial model was first minimized in vacuo using GROMACS 4.5 simulation package [28,29] using OPLS force field [30]. The vacuum minimized system was further subjected to 500 steps of steepest descent minimization in TIP3P water.

We considered the catalytic domain of the protein, BACE1, with residue number 1–385. We chose two different protein structures, PDB ID: 1FKN and 1W50. They differ greatly in flap orientation representing the closed and the open conformation of BACE1, respectively. All heteroatoms were removed from both the PDBs. In 1W50, there are missing residues in the region 160–169, far away from the active site cleft. This region was modeled using the SWISS-MODEL webserver [31] and the quality of the generated model was judged using ANOLEA and QMEAN analyses. Both 1FKN and modeled 1W50 were then minimized in vacuo followed by 500 steps of steepest descent minimization in TIP3P water using the OPLS force field.

2.2. Protein-peptide docking

To dock APP within the BACE1 active site, we used a protein-peptide docking procedure. Firstly, we used ClusPro 2.0 web-interface [32,33] to dock the APP fragment with BACE1. ClusPro uses a fast Fourier transform (FFT) based rigid body docking algorithm to explore all possible binding poses of the peptide within the active site by a systematic rotation and translation of the peptide. The best solution was selected based on visual inspection of the catalytic residues of BACE1 in close proximity to the cut-site of APP. The complex structure was further refined by flexible docking algorithm implemented in Rosetta FlexPepDock [34].

2.3. Molecular dynamics simulation

Conformational dynamics of both free BACE1 and BACE1–APP complex were studied using extensive molecular dynamics simulation with the aid of GROMACS 4.5 packages with OPLS force field. For free BACE1, we considered both 1FKN (closed) and 1W50 (open) PDB structures. Particular attention was given to the ionization state of the catalytic residue, the aspartate dyad (Asp32/Asp228). The optimal enzymatic activity of BACE1 is within the pH range of 3.5–4.5 where the catalytic dyad is probably mono protonated. We used Asp32 protonation and negatively charged Asp228 for BACE1 in accordance with the previous study [15]. We also considered the protonation of both the N-terminal and C-terminal amino and carboxyl groups of both BACE1 and APP.

Both free and APP bound BACE1 complex were subjected to a preliminary short energy minimization in vacuo using the steepest descent algorithm. Then the system was solvated with TIP3P explicit water model in a cubic box with periodic boundary condition. The box dimension was chosen such that all the protein atoms were at a distance equal to or greater than 10 Å from the box edges. The simulated system was made charge neutral by adding appropriate number of both Na^+ and Cl^- ions with ion concentration of 0.015 mol/lit. The solvated system was subjected to 1000 steps of energy minimization using steepest descent algorithm which is followed by 5000 steps of minimization using conjugate gradient algorithm. After that, a 100 ps position restrained dynamics was carried out where the protein/complex was restrained by adding restraining forces while the water molecules were allowed to move freely. It allows proper equilibration of solvent around the solute. It was then followed by 100 ps of NVT simulation at 300 K and 100 ps of NPT simulation to achieve proper equilibration of the system to be simulated. Final production simulations were performed in the isothermalisobaric (NPT) ensemble at 300 K, using an external bath with a coupling constant of 0.1 ps. The pressure was kept constant (1 bar) by using pressure coupling with the time-constant set to 1 ps. The LINCS [35] algorithm was used to constrain the bond lengths involving hydrogen atoms, allowing the use of 2.0 fs time step. Electrostatic interactions were calculated using particle mesh Ewald summation method [36]. Van der Waals interactions were truncated at 14 Å. The trajectories were stored at every 5 ps. Analyses were carried out with the trajectory analysis tools implemented in GROMACS.

To improve the sampling efficiency, we used a simple parallel sampling method where three uncoupled copies of the same system with different initial velocities assigned by using different seed number were simulated simultaneously. Thus each simulated system has three replicas and each replicate was simulated for 60 ns, thus producing a total of 180 ns of production simulation for each system. This method was successfully used to explore the conformational dynamics of a large protein, myoglobin, previously, with comparable simulation time scale [37].

2.4. Electrostatic surface potential analysis

Electrostatic surface potential of the BACE1–APP complex was analyzed by solving the Poisson–Boltzmann (PB) equation using PBEQ

solver implemented in the CHARMM–GUI interface [38,39]. The dielectric constant for protein core and solvent was considered as 1.0 and 80.0 respectively, with a salt concentration of 0.15.

2.5. Principal component analysis (PCA) and essential dynamics

PCA was then performed on the concatenated trajectories. All the replicas undergo conformational changes according to its environment within the initial period of the simulation after which each simulation achieves an equilibrium state. We, therefore, chose last 50 ns of each of the three replicas of a particular system and concatenated them to produce a production trajectory of 150 ns for each system.

Mass weighted covariance matrix of the Cα atomic positional fluctuations was calculated on the concatenated trajectory and essential subspace was then described by the variance retained by the reduced subspace defined by calculated eigenvectors. Essential dynamics of both free and complexed BACE1 were analyzed by the two extreme projections along the trajectory on the average structure corresponding to a particular PC and interpolate frames between the two extreme projections.

2.6. DynDom analysis

To identify large scale domain movement and hinge movement associated with protein dynamics, we have used the DynDom web-server [40]. Two extreme conformations generated from each trajectory, corresponding to PC1, were submitted to the web-server to determine protein domain dynamics, hinge axes and amino acid residues involved in the hinge bending.

3. Results and discussions

3.1. Recognition of APP by BACE1

To explore the recognition mechanism of BACE1 with APP, we have used a protein-peptide docking procedure. It is to be noted that initially we have considered both the open (PDB ID: 1W50) and closed (PDB ID: 1FKN) conformations of BACE1 for docking, but APP binds only to the open conformation and shows steric clashes while docked to the closed conformation. 1000 lowest energy solutions judged by a balanced scoring function are clustered and solutions from the 10 best clusters are reported. All the 10 BACE1–APP complexes have been visually inspected and the complex structure of 4th cluster has been selected as possible solution based on the prior knowledge of the presence of APP cut-site close to the catalytic aspartate dyad of BACE1 within the active site cavity. It is to be mentioned that although the complex belongs to the 4th cluster considering the size of the cluster, it ranks first considering the mean energy of the clusters. The complex structure has been further refined by flexible docking algorithm implemented in Rosetta FlexPepDock. The lowest energy solution has been selected from all the possible solutions and it shows 1.5 Å RMS deviations from the complex structure obtained from ClusPro 2.0. Structures of the BACE1–APP complex obtained from both ClusPro 2.0 and Rosetta FlexPepDock are shown in Fig. 1.

As evident from the figure, APP appropriately fits within the active site cavity of BACE1. The complex displays high steric compatibility in size and shape between the APP and BACE1 cavity, resulting in a tighter spatial fit of the peptide inside the cavity. The β-hairpin flap region tightly holds the peptide within the cavity. There is a kink at the cut-site residue of the APP which separates the N-terminal helix from the C-terminal helix. This kink is more prominent in the APP structure in the complex predicted by Rosetta FlexPepDock which allows a larger tilt in the C-terminal helix with respect to the N-terminal helical region of the APP. The orientation of the N-terminal helical region of the APP obtained from both the programs is highly similar as evident from the superimposed model shown in Fig. 1.

Nevertheless, the protein-peptide docking only allows a limited flexibility of the protein thus the large scale conformational switching induced by the bound peptide cannot be probed by docking algorithm. We therefore employed molecular dynamics simulation to exploit APP induced conformational changes of BACE1 and also to obtain a refined BACE1–APP complex.

3.2. Molecular dynamics simulation

The APP induced conformational switching of BACE1 has been probed by molecular dynamics (MD) simulation using GROMACS packages [28,29] for both free and APP bound BACE1 obtained from docking studies. To study the dynamics of substrate free BACE1, we have considered two distinct initial conformations, 1FKN (closed) and 1W50 (open) respectively. These two conformations of BACE1 largely differ in the flap orientation.

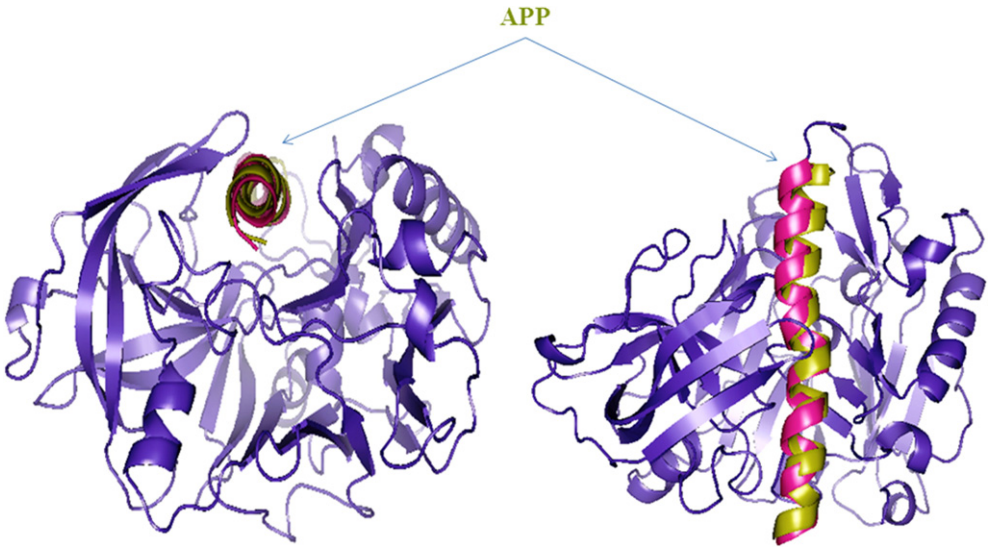

Fig. 1. Structures of the BACE1–APP complex obtained from molecular docking study in cartoon representation. BACE1 is colored blue whereas the bound APP is colored yellow (ClusPro 2.0) and pink (Rosetta FlexPepDock).

3.2.1. Dynamics of free BACE1

Fig. 2 depicts the variations of two global structural parameters — root mean square deviation (RMSD) and radius of gyration (R_g) of the closed and open BACE1 conformations with simulation time for three replicas. Differential distributions of both the RMSD and R_g profile for all the three replicas of each of the simulated systems indicate that the conformational subspace defined by each replica for a particular system is significantly different from the others. It has been well documented that simulations starting from the same initial structure but with different initial velocity distribution, sample different direction of conformational space during the simulation [37].

The RMSD of the backbone Cα atoms of the simulated protein over time can be used to evaluate the structural stability of the system. Fig. 2A reveals that both in case of closed and open conformation, all the replicas undergo conformational changes according to its environment within the very first nanosecond of the simulation and after that each simulation achieves equilibrium state as evident from the stable RMSD profile. For the closed conformation, the average Cα-RMSD fluctuations are 0.14 ± 0.026 nm, 0.165 ± 0.037 nm and 0.17 ± 0.039 nm with respect to the initial conformation of BACE1 for replicas 1, 2 and 3 respectively. While for the open conformation, the average Cα-RMSD are 0.23 ± 0.02 nm, 0.26 ± 0.03 nm and 0.18 ± 0.028 nm with respect to the initial conformation of the protein for replicas 1, 2 and 3 respectively.

On the other hand, R_g provides insight into the overall dimension and shape of the protein. The plot of R_g versus simulation time is shown in Fig. 2B. Overall stable Rg profile observed for both closed and open BACE1 simulations indicates no structural instability or uncoiling. Comparison of the R_g profile for 1FKN and 1W50 reveals that the latter shows more fluctuation which is in accordance with the RMSD profile that indicates larger sampling of diverse conformational spaces for 1W50 simulation compared to 1FKN simulation.

We then analyzed the fluctuation of each residue of BACE1 during the simulation and the variation of root mean square fluctuation (RMSF) of each residue is shown in Fig. S1 (Supplementary material 1).

Interestingly, regardless of the initial conformation of the protein that is either open or closed, all the simulations exhibit similar RMSF variation profile. Careful observation of the regions of high fluctuation reveals that the flap region shows significant fluctuation during the simulations. Particularly GLN 73 shows highest RMSF values among all the flap residues. Besides the flap residues, there are several other short loopy segments that frame the active site cavity of BACE1 that also exhibit high fluctuation during the simulation, as evident from the RMSF profile. These regions are “10s loop”, “A loop”, “F loop” and “D loop”. A schematic representation of the position of each loop in the BACE1 cavity is shown in Scheme 1B. These regions frame the extreme C-terminal lining of the active site cavity of BACE1. Concerted movements of these entire loop regions can lead to significant conformational changes in the active site cavity of BACE1.

3.2.2. Dynamics of the BACE1–APP complex

We have also investigated the stability of the docked BACE1–APP complex using MD simulation with three replicas of the complex, each with a time scale of 60 ns and the results have been summarized in Fig. 3.

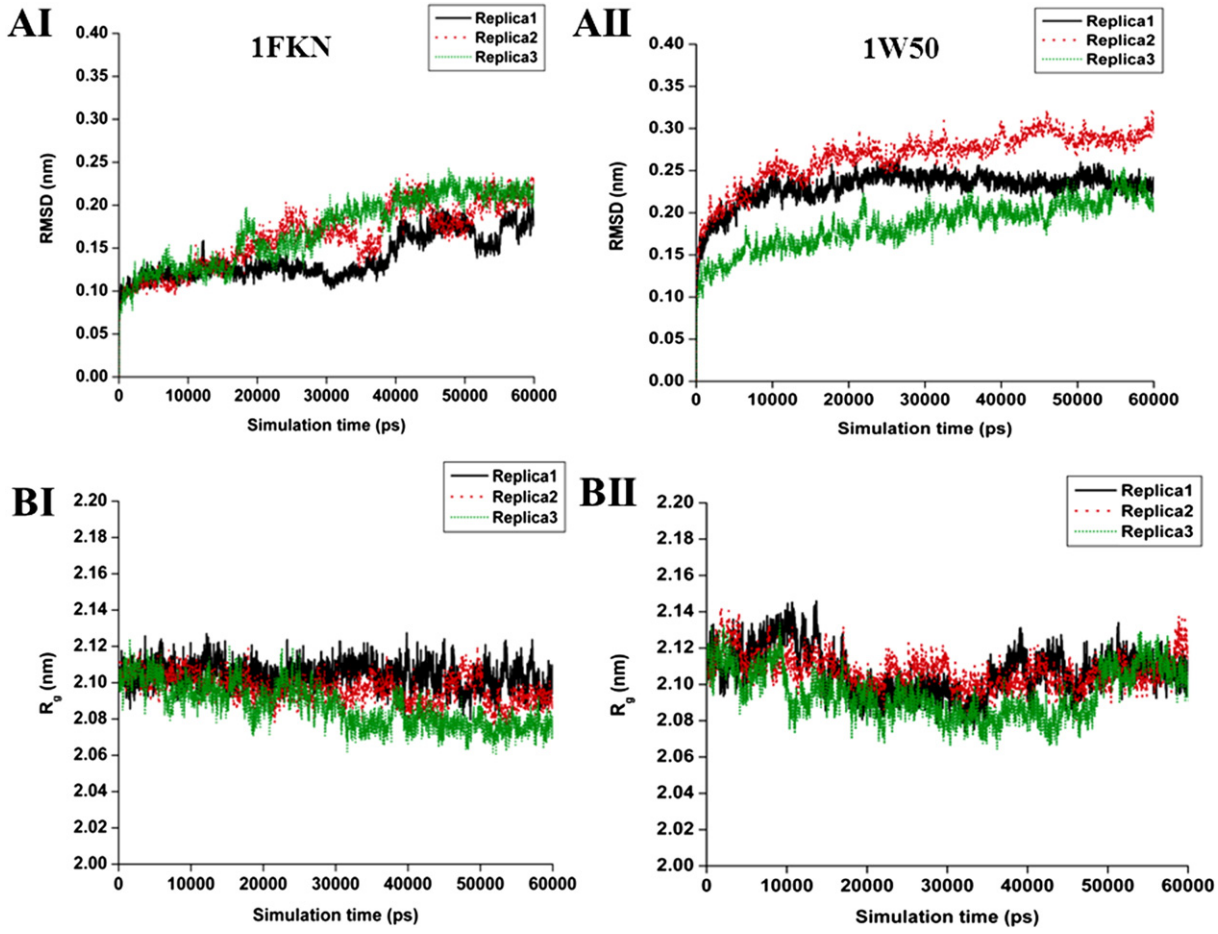

Fig. 2. Variations of RMSD (A) and Rg (B) with simulation time for free BACE1 obtained from molecular dynamics simulation. Left panel represents results obtained from 1FKN simulation (I) whereas right panel represents result obtained from 1W50 simulation (II). 1FKN and 1W50 represent the “closed conformation” and the “open conformation” of BACE1, respectively.

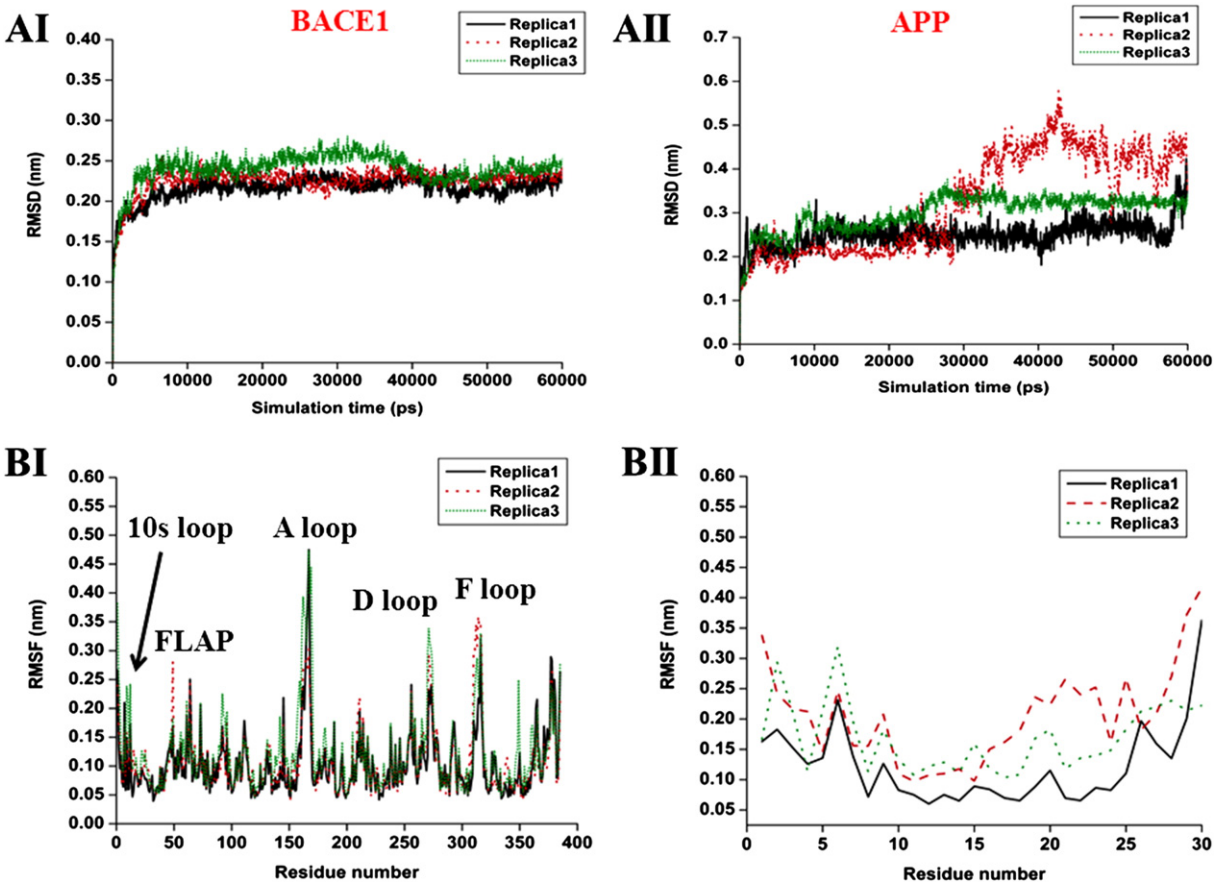

Fig. 3. Variations in RMSD of BACE1 (AI) and bound APP (AII) during the simulation of the BACE1–APP complex. Variations in RMSF of BACE1 (BI) and bound APP (BII) during the simulation of the complex.

Fig. 3 AI displays the RMSD variations of the Cα atoms of the BACE1 in the complex. The RMSD profiles for all the three replicas are highly stable throughout the simulation time indicating proper equilibrations of the simulated systems. Also it is to be noted that the RMSD profile of BACE1 in the complex is highly stable than the free protein indicating confinement in a stable conformational state upon complex formation. On the other hand, a significant change is observed in the RMSD profile of APP in the complex. The highly fluctuating RMSD profiles indicate conformational changes during the simulation. Particularly, replica 2 is more flexible than the other two replicas (Fig. 3 AII). After 30 ns, the RMSD changes from 0.24 to 0.5 nm although for the remaining simulation it fluctuates within 0.4 to 0.5 nm. A closer look in the trajectory reveals that the C-terminal region of the bound APP undergoes structural transition. The kink is more pronounced and the C-terminal helix moves laterally with respect to the N-terminal helix. Residue wise fluctuations reveal that BACE1 in complex exhibits similar fluctuation pattern when compared to free BACE1. The loopy segments in the active site cavity e.g. 10s loop, A loop, D loop and F loop are also found to be flexible during the simulation for the complex. In contrast to the free BACE1 dynamics, the flap region is more stable when BACE1 is complexed with APP (Fig. 3 BI). Another interesting observation is the altered fluctuation of the F loop. In BACE1–APP complex the loop is less flexible compared to the free BACE1. On the other hand, the bound APP exhibits high fluctuation during the simulation with the C-terminal helical region displaying more flexibility than the N-terminal region. The APP cut-site at the middle is highly stable (Fig. 3 BII). Flap region tightly retains the APP cut-site in close proximity to the aspartate dyad and the orientation remains stable throughout the simulation.

3.2.3. Flap orientation in free and complexed BACE1

BACE1 is known to possess two distinct conformational states, namely the open and the closed conformation. These two conformational states are mainly differing on the basis of the orientations of the β-hairpin flap region which covers the active site of the protein. We thus carried out a detailed analysis of the flap orientation in both free and APP bound BACE1.

Fig. 4A reveals the variation of RMSD of the flap region for all the three replicas of each simulation. For both the free BACE1 simulations i.e. either starting with a closed conformation (1FKN) or an open conformation (1W50), the flap RMSD never stabilizes. It fluctuates in between the RMSD of 0.10–0.25 nm with respect to the initial conformation. This behavior indicates that the flap region in substrate free BACE1 shows high mobility and can access different conformations during the simulation. On the other hand, RMSD profile of the flap region in BACE1–APP complex is confined within a narrow conformational space indicating attainment of stability upon complex formation.

Fig. 4B represents the RMSD distribution of the flap region for all the three systems. We have concatenated the last 50 ns of all the three replicas of each simulating system to analyze the flap RMSD distribution. For free BACE1, irrespective of the initial conformation either closed (1FKN) or open (1W50), there is a bimodal distribution. The first peak appears at ~0.1 (nm) and the main peak appears at ~0.18–0.2 nm with respect to the initial conformation of the flap region. It is to be noted that in both the simulations for free BACE1, although the number of conformations in a particular population are different but the peak positions are fixed. This feature indicates that the flap region in the substrate free BACE1 appears in two distinct conformational spaces during the simulation. On the contrary, when APP is bound to BACE1, we found

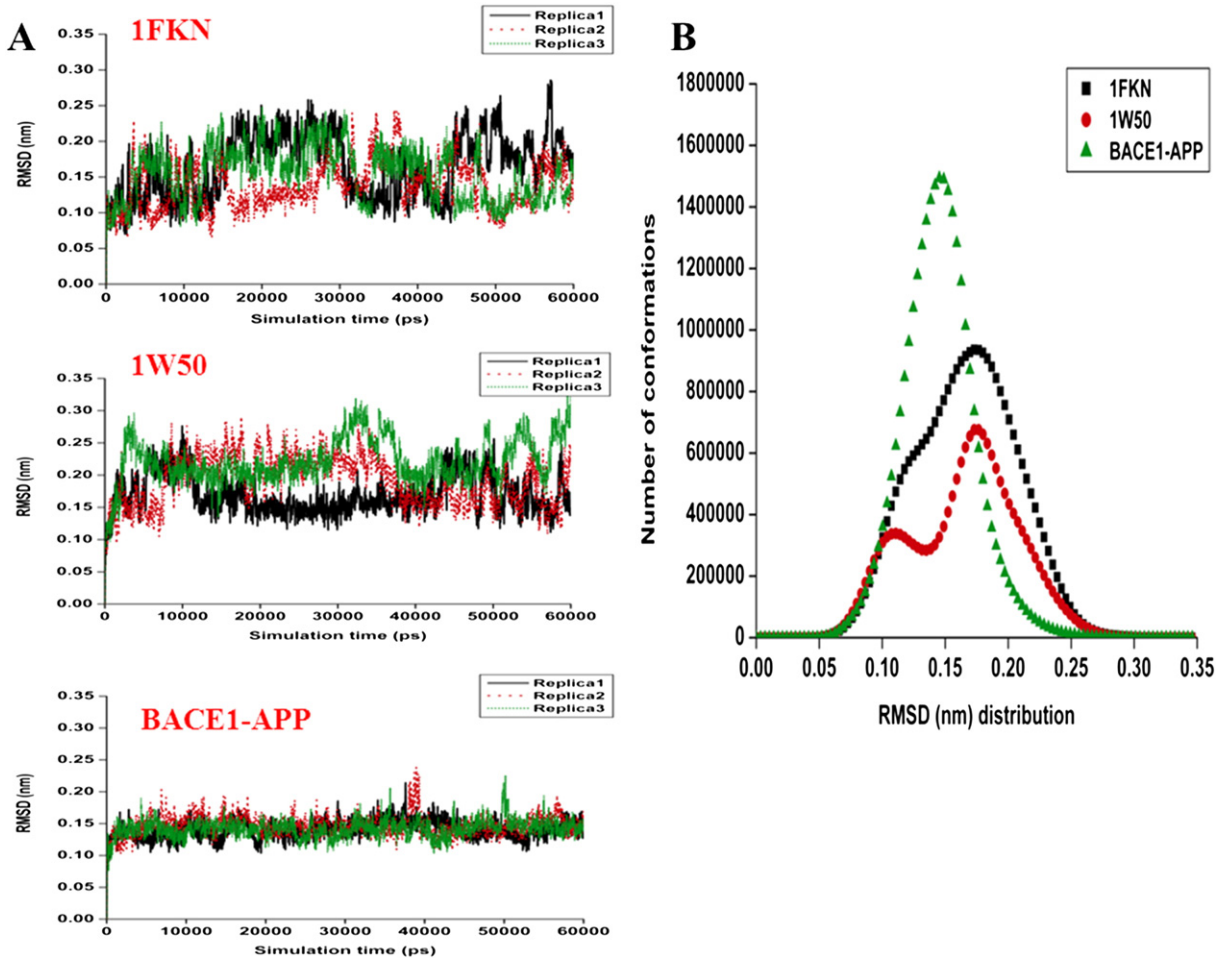

Fig. 4. A: Variations of Cα RMSD of the flap region for all the three replicas for each of the three simulations, two free BACE1 simulations — one starting with a closed conformation (1FKN) another with an open conformation (1W50) and BACE1–APP complex. B: RMSD distribution of the flap region in all the three simulations.

a single population of flap conformation in the concatenated trajectory, that has an RMSD of ~0.15 nm with respect to the initial structure indicating confinement in a single conformational space during the simulation.

3.2.4. Analysis of cavity opening during the simulations

We have further analyzed the degree of cavity opening in both free and APP bound BACE1. It is to be noted that the separation between

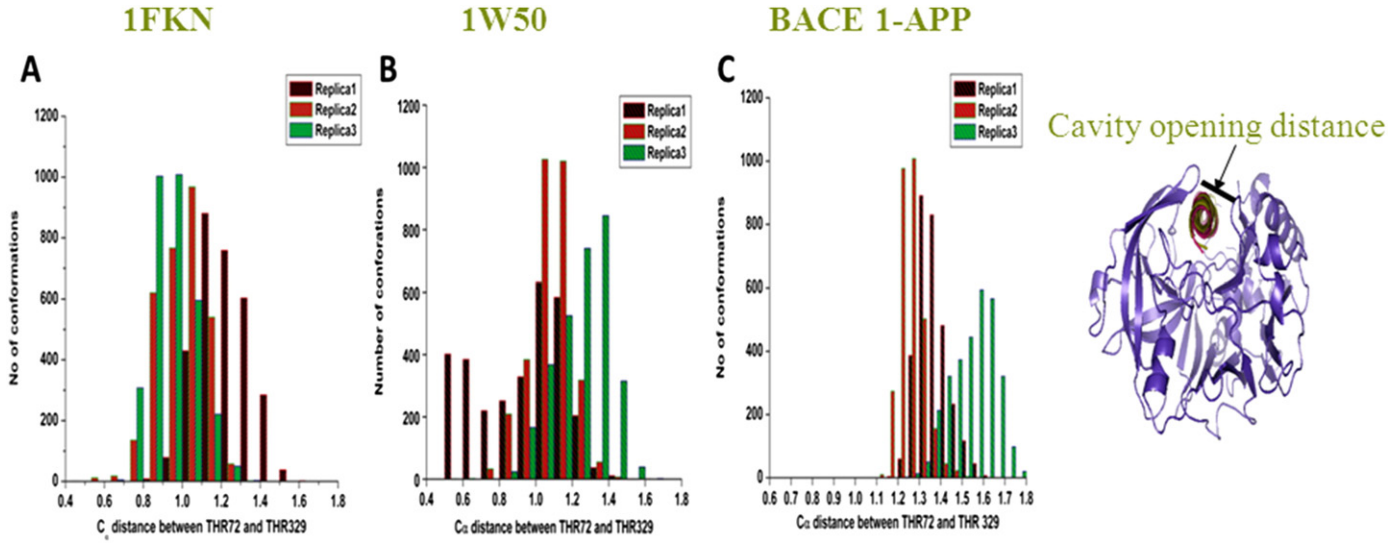

Fig. 5. Histogram representations of the Cα distances between THR72 and THR329 of all the three replicas for each of the three simulations, two free BACE1 simulation — one starting with a closed conformation (1FKN) another with an open conformation (1W50) and BACE1–APP complex. Pictorial representation of the cavity opening is shown in the extreme right panel of the figure.

THR72 at the flap region and THR329 at the other side of the active site cleft has been previously used as a criterion for flap opening [18]. Histogram representations of the Cα distances between THR72 and THR329 of all the three replicas for both free (1FKN and 1W50) and APP bound BACE1 have been shown in Fig. 5.

In case of free BACE1 simulation starting from a closed conformation, the cavity opening distance is confined within the range of 0.8 nm to 1.4 nm (Fig. 5A). In case of replica 1 of 1FKN, BACE1 mostly visits conformations with wider active site cavity opening in the range of 1.0 nm to 1.4 nm with a peak at 1.15 nm. For replica 2, the cavity opening is further squeezed within 0.8 nm to 1.25 nm with the peak at ~1.1 nm. Very small population of closed conformation characterized by very small cavity opening distances (0.5–0.7 nm) also has been observed during the simulation. In the third replica of 1FKN, the cavity opening distances are mostly confined within narrower range of 0.8 nm to 1.2 nm with the peak at 0.9 nm and 1.0 nm. In contrast, for free BACE1 (1W50), the cavity opening distances are widely distributed from very narrower cavity opening to a wide cavity opening (Fig. 5B). Particularly for the first replica of 1W50, the cavity opening distances are widely distributed from 0.5 nm to 1.4 nm. There is a considerable population of conformations with very short cavity opening (0.5 nm to 0.7 nm) while most of the population have a cavity opening distance of 1.0 nm to 1.1 nm. The second replica is mostly confined within a narrower region of cavity opening distances, sharing the peak with replica 1. For the third replica, the protein mostly visits conformations with wider cavity opening. Most of the conformations are relatively open conformation with the cavity opening distances lying within 1.2 nm and 1.6 nm. Thus for free BACE1 simulation, the protein can visit a widespread region of cavity opening distances from too short to a wide cavity opening.

When APP is bound to the protein, the cavity opening distances of the complex are distributed within a narrower region (Fig. 5C). During the first and second replica of the simulations, most of the conformations exhibit cavity opening distances between 1.2 nm and 1.35 nm, whereas during the simulation of the third replica of the complex, the cavity opening widens up with the distance ranging from 1.4 nm to 1.7 nm. It is to be noted that in the complex, the bound substrate is a peptide and therefore renders a wider volume within the cavity. Conformations with shorter cavity opening distances as observed in the free protein have not been observed during the simulation of the bound protein.

3.2.5. Cluster analysis of the flap region

To gain a detailed insight into all the visited conformations of the flap region during MD simulation for free and APP bound BACE1, we have performed cluster analysis and the results are displayed in Fig. S2 (Supplementary material 1).

Clustering has been performed on the concatenated trajectories of 150 ns of each of the three simulations, free BACE1 starting with closed conformation (IFKN), open conformation (1W50) and BACE1–APP complex. Flap conformations have been clustered considering a stringent RMSD cutoff of 0.1 nm using the GROMOS clustering algorithm. Analysis on the concatenated trajectories of free BACE1 starting from closed (1FKN) and open (1W50) conformation results in 108 and 81 clusters of flap conformations respectively, whereas the BACE1–APP complex resulted in 55 clusters of flap conformation. This signifies that the flap region is more flexible in free BACE1 than in the BACE1–APP complex.

Fig. S2A reveals population distributions of the top 20 clusters of all the three simulated systems. 41% and 46.5% of the flap conformations of closed and open trajectory, respectively, are confined within the first three clusters whereas, 68.5% of the flap populations of the concatenated trajectory of the BACE1–APP complex simulation are confined in three most populated clusters. Structural overlay of the cluster average conformation of the flap region from top 20 clusters of each of the three simulated systems (open, closed and BACE1–APP complex) have been displayed in Fig. S2B, C and D respectively. Flap tip region is highly flexible in both free BACE1 structures. Particularly, the side-chain orientations of the THR72 residue in free BACE1 are widely distributed whereas when BACE1 is bound to APP, it is confined within a narrower space in 3-D. Thus the flap tip is less flexible in BACE1–APP complex. Another important observation involves the orientation of TYR71 and TRP76. In both the free BACE1 simulations, these two residues are more flexible whereas in complex the side-chains of these two residues are more confined indicating their involvement in specific interactions with bound APP.

3.2.6. Principal component analysis and essential dynamics

To identify large scale collective motions observed during MD simulation, we have applied principal component analysis (PCA) followed by essential dynamics analysis. PCA is essentially a data reduction technique where the atomic positional fluctuation matrix obtained from MD simulation has been diagonalized to obtain the eigenvectors and its corresponding eigenvalues. Then the eigenvectors are arranged in the descending order of the associated eigenvalues. Dynamics of the protein is now defined by the eigenvectors in the reduced subspace. Furthermore, the principal motions in the essential subspace can be inspected by projecting the protein along each component (PCs). 3465 eigenvectors are needed to define the variance observed in the MD simulation for each of the concatenated trajectories. Eigenvalues associated with each PC reveals that the first few components are more informative compared to the latter which carries very little information about the protein dynamics. Overall flexibility of the protein can also be inferred by the trace of the diagonalized covariance matrix of the Cα atomic positional fluctuations. Trace of the covariance matrix value obtained for the BACE1–APP complex is lower than that of free BACE1 (closed and open) indicating reduction of flexibility of the protein upon complex formation.

2-D projections of the first two PCs (PC1 and PC2) on the concatenated trajectories of free BACE1 either starting from closed or open conformation and only BACE1 in BACE1–APP complex are shown in Fig. 6A. Here, each point in the essential sub-space defines a unique conformation of the simulated system such that structurally similar conformations overlap in the essential sub-space. The concatenated trajectory of BACE1 starting from a closed conformation is highly flexible and visits numerous distinct conformational states as evident from a widespread projection distribution in essential space constituted by first two PCs (Fig. 6). Open conformation of BACE1 exhibits relatively less flexibility during the simulation and occupy three distinct conformational spaces.

Detailed analysis reveals that each of these three different clusters in essential subspaces is obtained from each of the three replicas of the simulated systems. Interestingly, the dynamics of the protein when in complex with APP are confined in three distinct population clusters with highly reduced spatial distribution in essential subspace indicating a reduction in the flexibility of the protein upon complex formation with APP. Another interesting observation is that in essential subspace, the behavior of BACE1 in complex, is similar to the dynamics of open BACE1 which is distinctively different from the dynamics of closed BACE1 and there is a substantial overlap in the conformational space between BACE1 in complex and starting with an open conformation (1W50). This can be attributed to the similarity in the cavity opening controlled by the flap region and its opposite loop. Fig. 5 reveals that during both the simulations with free BACE1, the protein in the open structure mostly visits wider cavity opening conformations while in the closed structure, there is a considerable population of conformations with narrower cavity opening.

In Fig. 6B, we have compared the conformational dynamics of BACE1 only in complex and the BACE1–APP complex in the reduced bi-dimensional subspace. The difference in the projection is due to the dynamics of the bound APP. As evident from the figure, first and third replica of both the simulations occupy very similar conformational cluster but behavior of both the systems are different in case of the second replicate, wherein the BACE1–APP complex is more flexible as

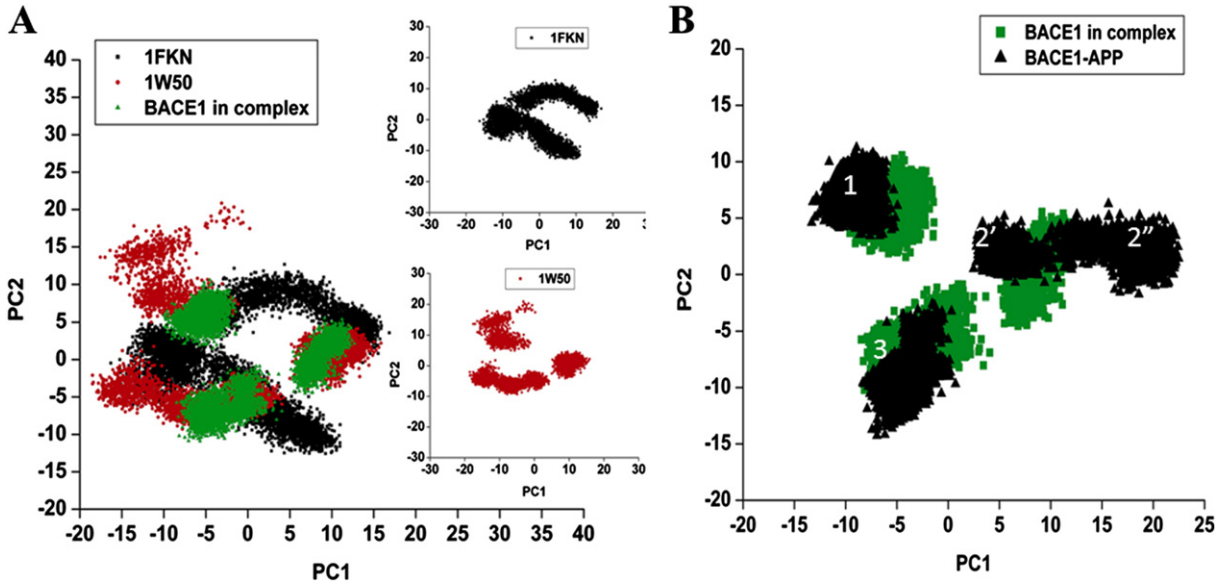

Fig. 6. Principal component analysis obtained from MD simulations. A: 2-D projection of BACE1 in bi-dimensional subspace defined by the first two PCs (PC1 and PC2) on the concatenated trajectories of three simulations, 1FKN simulation (black), 1W50 simulation (red) and BACE1–APP complex (green). 1FKN and 1W50 represent the "closed conformation" and the "open conformation" of BACE1, respectively. For clarity the 2-D projections of 1FKN simulation (black), 1W50 simulation (red) are also shown in inset, separately. B: 2-D projections of BACE1 (green) and BACE1–APP complex obtained from the concatenated trajectory of BACE1–APP complex. 1, 2 and 3 represent 1st, 2nd and 3rd replica of the BACE1–APP complex simulation, respectively. 2′ and 2″ in the figures indicate the bi-dimensional projections of the second replicate during the 1st and 2nd half of the simulation, respectively.

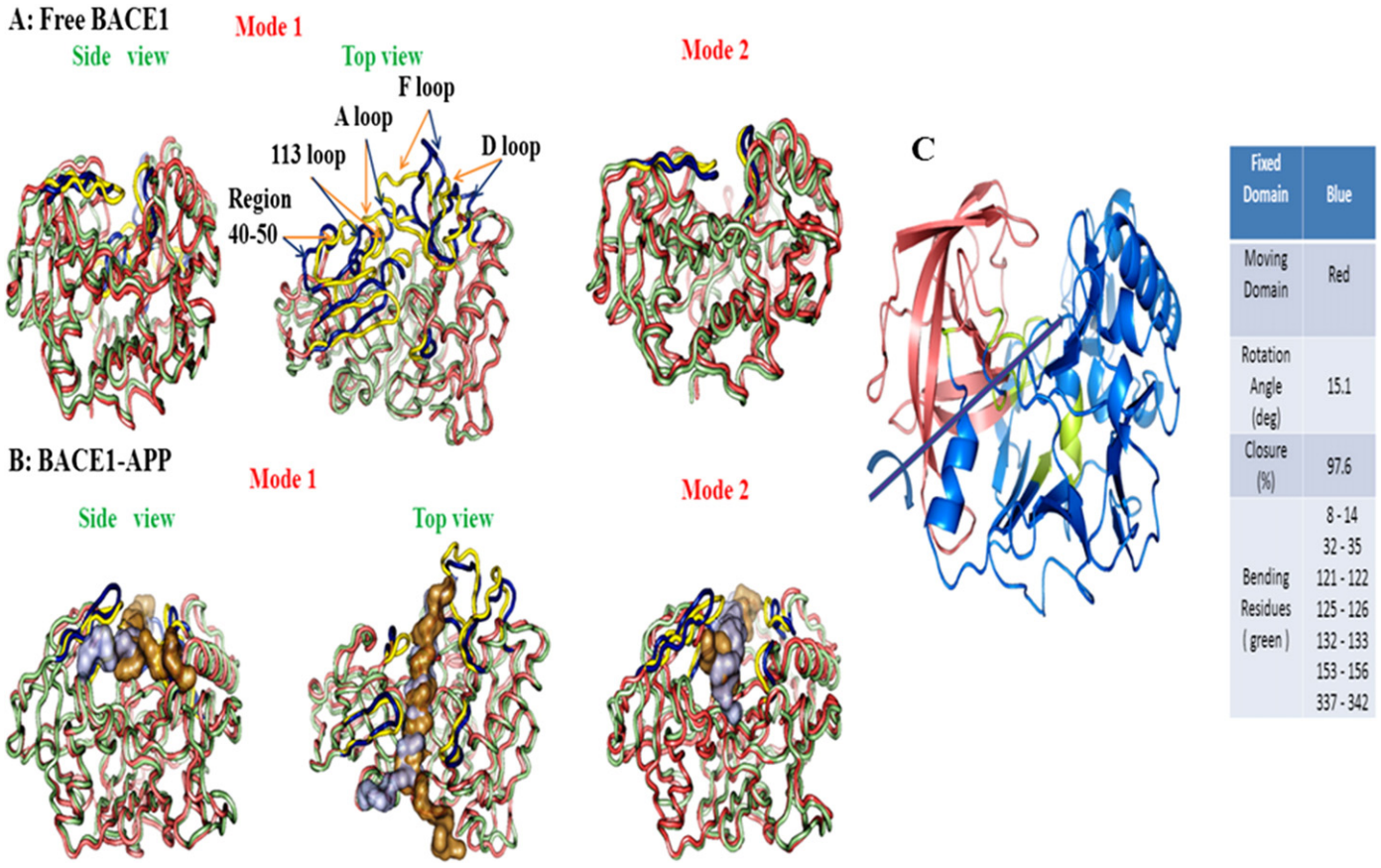

Fig. 7. Essential dynamics of free BACE1, 1FKN (A) and BACE1–APP complex (B) obtained from MD simulation. Two extreme conformations of the simulated systems are colored as deep salmon and green. Regions of the active site showing high deformation have been colored separately. Yellow and blue color represent regions of high deformations on the two conformations of BACE1 colored in deep salmon and green respectively. C: Cartoon representation of the domain movement of free BACE1 using DynDom web-interface. Bending residues are colored green and the rotational axis is shown by the arrow.

evident from a widespread projection distribution. This is attributed to the high conformational dynamics of bound APP also supported by the high RMSD profile (Fig. 3AII). 2′ and 2″ in the figures indicate the bi-dimensional projections of the second replicate during the 1st and 2nd half of the simulation, respectively. As evident from the projection, two halves of the simulation of the second replicate of the complex occupies distinct conformational subspace due to differential conformational dynamics of bound APP.

3.2.7. Biologically relevant collective motion

In general, biologically relevant motions of a macromolecule are associated with long-timescale domain motions and can be described by large-amplitude collective motions of the macromolecule. First two PCs of every simulated systems show maximum collectivity and can explain most of the dynamics observed during the simulation. We thus studied the dominant motions that occurred during the MD simulations by generating the two extreme projections along the MD trajectory on the average structure for both PC1 and PC2 (Fig. 7). The first PC represents the most dominant motion during the MD simulation.

Two extreme conformations of the simulated systems have been obtained by projecting the system along the eigenvector of a particular PC and colored differently (deep salmon and green). Regions of the active site showing high deformation have been colored separately. Yellow and blue color represent regions of high deformations on the two conformations of BACE1 colored in deep salmon and green, respectively. It is to be noted that in both the free BACE1 simulations, the observed motions corresponding to a particular PC are same. Therefore, we represent the motion observed in 1FKN simulation as free BACE1 simulation. Motions of free BACE1 along PC1 reveal primarily the movement in active site regions (Fig. 7A). Particularly, the bottleneck of the active site cavity framed by two flap regions, tip of the flap region comprising residues 67–77 and the other loop region comprising residues 327–330 in the opposite site of the flap, undergo significant concerted motion towards each other leading to cavity closing. Top view of the protein reveals high flexibility in other loopy segments that frames the active site cavity of BACE1. In particular, concerted movements in the F loop (311–316), the D loop (270–273) and A loop (158–167) that lines the extreme C-terminal cavity shows high deformation during the simulation. All these loop regions move towards the aspartate dyad and facilitate the transition from open to closed conformation of the protein.

The short '10s loop' (residues 9–14) located between two strands at the base of the catalytic pocket also moves significantly during the simulation. It is to be noted that these regions show high disorder in all of the X-ray structures of BACE1 [9,11,12] and also exhibit high $<R^2>$ values as calculated in our recent NMA study [10]. Interestingly, region 40–50 of BACE1 and another loop segment comprising of residue 104–114, known as "113 loop", moves significantly towards the aspartate dyad. Movements of these entire loop regions towards the active site in association with lateral movement of the flap region and its opposite loop towards each other further squeeze the cavity indicating a conformational transition of the protein from open to closed form. Cavity volume calculation reveals that concerted movement of these loops and flap region reduce the cavity volume from 978.94 Å3 to 464.70 Å3, again reconfirming open to closed conformational transition. On the other hand, motion of free BACE1 along the second PC (PC2) reveals very similar movement in same regions as observed for PC1 but the amplitude of the motion is much less and the type of motion in the flap region is different. The flap region and its opposite loop show up and down movement rather than the lateral movements observed for PC1.

BACE1–APP complex exhibits different types of motion in essential sub-space. Movement of the complex along PC1 reveals primarily movement of the bound APP, shown by surface representation (Fig. 7B). The C-terminal region of the bound APP shows high lateral movement which induces a kink at the cut-site residue of the APP. This motion has been also observed in the APP structure of the complex predicted by Rosetta FlexPepDock (Fig. 1). BACE1, on the contrary, appears far more rigid in the complex. The cavity opening framed by the flap and its opposite loop region moves towards each other and also exhibit downward movement towards APP. This movement allows flap region to tightly retain the APP in the active site of the BACE1. Also flexibility has been observed in the D loop, F loop and 113 loop regions. All these loops move towards the bound APP, thus allowing maximum surface complementarity between the receptor and bound APP. These concerted movements facilitate APP to tightly bind in the BACE1 cavity forming a BACE1–APP closed complex. Motions of BACE1–APP complex along PC2 reveals concerted movement of the flap region and its opposite loop and a portion of D loop towards the bound APP.

3.2.8. Analysis of domain movement

We performed DynDom analysis [40] on the two extreme conformations of the trajectory for both free BACE1 and BACE1–APP complex generated by projecting them along the first PC. DynDom predicts domain movement associated with a hinge motion for free BACE1, but does not predict any hinge movement for BACE1–APP complex. Result of DynDom analysis has been summarized in Fig. 7C.

DynDom predicts hinge movement between two domains comprising of 264 residues (blue, fixed domain) and 117 residues (red, moving domain). Bending residues are colored green and the rotational axis is shown by the arrow. There is a 15.1° rotation around the hinge axis which moves one domain with respect to the other domain. It is to be noted that the "10s loop" and a part of "A loop" are the part of bending residues that allow the hinge movement of the two domains of free BACE1.

3.2.9. BACE1–APP interaction analysis

We then analyzed the essential interaction responsible for APP recognition by BACE1. PCA analysis on the trajectory of BACE1–APP complex is distributed in three different conformational clusters, so we have chosen a representative conformation of the complex from each cluster as an ensemble representative. Protein peptide interactions have been analyzed in all the three complex structures and shown in Fig. 8 and Table S1 (Supplementary material 2).

Fig. 8A reveals the van der Waals interactions between APP and BACE1. In the N-terminal helix of APP, strong van der Waals interactions have been observed between LEU 2 and ILE 5 of APP with LEU 267 and VAL 309 of BACE1 respectively, while ILE 10 interacts with one of the "113 loop" residue ILE 110. TYR 71 of the "Flap region" tightly retains the APP to the active site by interacting with ALA 17 of APP that is close to the cut-site. PHE 19 of APP tightly fits into the groove formed by the three residues of BACE1, i.e., TYR 198, ILE 226 and VAL 332.

Fig. 8B shows electrostatic interactions between BACE1 and APP. As evident from the electrostatic surface potential of BACE1, the protein is highly charged and contains specific regions of positively and negatively charged surfaces. Specific electrostatic interactions between APP and BACE1 facilitate binding. The N-terminal region of the APP binds into a region of strong positive electrostatic potential. Particularly, two negatively charged residues GLU 9 and GLU 11 show strong electrostatic interaction with LYS 321 of BACE1. A specific electrostatic interaction between LYS 6 of APP and GLU 265 also has been observed in this region. Just after the cut site of APP, ASP 16 forms strong interaction with ARG 235 and this interaction is very crucial to appropriately orient the cut-site of APP towards the catalytic ASP dyad. On the other hand, two acidic residues GLU 18 and ASP 22 of APP are electrostatically clamped with ARG 128 of BACE1. There is a strong electrostatic interaction between the extreme C-terminal residue HIS 29 of APP with a region of strong negatively charged surface, primarily contributed by ASP 130 of the receptor. In addition there are π-stacking aromatic interactions and also π-cation interactions in the BACE1–APP complex (Fig. 8C). TYR 198, of BACE1 shows stacking interaction with another aromatic residue, PHE 19, of APP. On the other hand, LYS 14 residue just before the cut site is involved in π-cation interactions with two aromatic

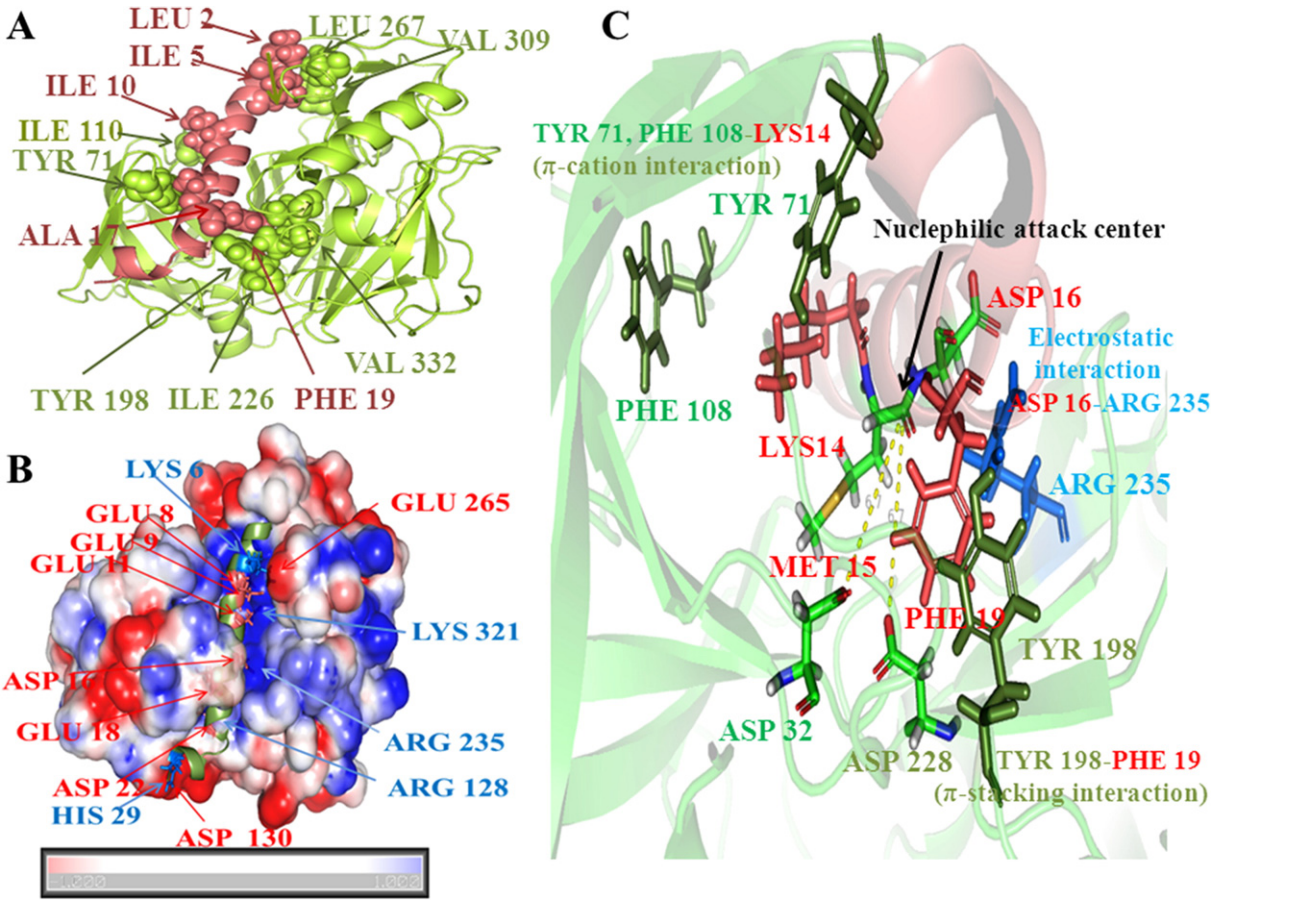

Fig. 8. Details of the interactions involved in APP recognition by BACE1. A: Details of the van der Waals interactions between APP and BACE1. Interacting residues are shown in CPK representations. BACE1 and APP are colored as lime-green and salmon color. B: Electrostatic surface potential of BACE1 when APP is bound to BACE1. Regions of positively and negatively charged surface area are colored in blue and red color. C: Details of the π-cation and aromatic stacking interactions between BACE1 and APP in complex. Interacting residues are rendered in stick representation. The distance between catalytic aspartate dyad and the Carbonyl Carbon between MET 15 and ASP 16 where the nucleophilic attack happens is shown as dotted line. Electrostatic clamping observed between ASP 16 of APP and ARG 235 of BACE1 is rendered in stick representation.

residue TYR 71 and PHE 108 of BACE1. It is to be noted that there is no direct interaction between catalytic aspartate dyad and the carbonyl carbon between MET 15 and ASP 16 where the nucleophilic attack happens during catalysis. The distance is 6.7 Å from aspartate oxygen to the nucleophilic carbon center. It is well documented that the nucleophilic attack is mediated through a water molecule [15,19]. But electrostatic clamping between ASP 16 of APP (residue just before the cut-site) and ARG 235 appropriately orients the cut-site towards the catalytic dyad thus facilitating the nucleophilic attack.

We have also analyzed the hydrogen bonding interactions between BACE1 and APP in all the three complex structures obtained from three different population clusters using PIC web-server [41]. Details of hydrogen bonding interactions between APP and BACE1 are shown in Table S1 (Supplementary material 2). Particularly, in all the three complexes, the flap region interacts strongly with the APP through a hydrogen bonding interaction involving TYR 71. It is to be noted that TYR 71 of the flap region of BACE1 is also involved in both van der Waals as well as π-cation interaction with the bound APP and tightly retains the APP at the active site. This is supported by the observation that in the BACE1–APP complex, TYR 71 is less flexible compared to free BACE1 (Fig. S2). ARG 128 is another important residue of BACE1 that is involved in several hydrogen bonding interactions with APP. ASN 233 is also involved in a strong hydrogen bonding interaction with GLU 12 of APP. Two more residues in the "F loop" (ARG 307 and LYS 321) are also involved in several hydrogen bonding interactions with APP.

4. Conclusions

Here, we have explored the structural details of the conformational switching of BACE1 during APP recognition using all-atom molecular dynamics simulation. Our simulation indicates APP recognition by BACE1 to be a conformation selection process. PCA and essential dynamics reveal that free BACE1 is highly flexible and can access different conformations in essential subspace. High fluctuations have been observed in several loop regions that line the active site cavity of BACE1 along with the flap region that frames the cavity opening. Concerted movements of all these regions lead to a conformational transition from open to closed form of BACE1. During simulation, free BACE1 visits both open and closed forms. Cavity opening distance distribution reveals that during the free BACE1 simulation, conformations with both short and large cavity opening are observed. While, upon complex formation with APP, the flexibility of BACE1 reduces significantly, particularly, the flap region. The RMSD distribution of the flap region in the complex indicates confinement in a single population of conformation. Essential dynamics reveals that the flap and its opposite loop region move towards each other and also the D loop, F loop and 113 loop regions move towards bound APP, thus allowing maximum surface complementarity between the receptor and bound APP. All these concerted movement enable APP to tightly bind in the BACE1 active site cavity forming a BACE1–APP closed complex thus proposing a conformational selection hypothesis for APP recognition by BACE1.

Principal component analysis along with cluster analysis reveals that the flap region is highly flexible during free BACE1 simulation while upon complex formation, the mobility of the flap region significantly reduces. The flap region interacts strongly with the bound APP particularly involving TYR 71 through hydrogen bonding, van der Waals as well as π-cation interaction with APP thus retaining it in the active site and appropriately orienting the cut-site to facilitate proteolysis. Sequence analysis of β-cleavage site in APP reveals that BACE1 possesses specificity for a negatively charged residue at P1′ site (residue just before the cut-site) [25]. Electrostatic surface potential for the BACE1–APP complex clearly illustrates that the P1′ site binds into a region of strong positive electrostatic potential which rationalize the sequence preference of the β-cleavage site.

Results obtained from molecular dynamics simulation indicate novel insight into the mechanism of APP recognition by BACE1. We also explored the specific interaction necessary for APP to bind to the active site of BACE1, the information that can be further extended to design more potent inhibitors in Alzheimer's Disease.

Supplementary data to this article can be found online at http://dx.doi.org/10.1016/j.bpc.2015.03.006.

Acknowledgments

SB gratefully acknowledges the financial support from the Department of Science and Technology (Govt. of India, Ref No: SR/SO/BB-0105/2010, dated: 20/06/2012). The authors gratefully acknowledge BIOGENE high performance computing facility at the Bioinformatics Resources and Applications Facility (BRAF) and the Centre for High Performance Computing for Modern Biology, Ballygunge Science College, University of Calcutta for providing us computational facility.

References

[1] J. Hardy, D.J. Selkoe, The amyloid hypothesis of Alzheimer's disease: progress and problems on the road to therapeutics, Science 297 (2002) 353–356.
[2] D.J. Selkoe, The molecular pathology of Alzheimer's disease, Neuron 6 (1991) 487–498.
[3] D.M. Walsh, D.J. Selkoe, Aβ oligomers — a decade of discovery, J. Neurochem. 101 (2007) 1172–1184.
[4] D.J. Selkoe, Cell biology of the amyloid beta-protein precursor and the mechanism of Alzheimer's disease, Annu. Rev. Cell Biol. 10 (1994) 373–403.
[5] G. Thinakaran, E.H. Koo, Amyloid precursor protein trafficking, processing, and function, J. Biol. Chem. 283 (2008) 29615–29619.
[6] G.X. Lin, S.W. Koelsch, D. Downs, A. Dashti, Human aspartic protease memapsin 2 cleaves the β-secretase site of Aβ-amyloid precursor protein, Proc. Natl. Acad. Sci. 97 (2000) 1456–1460.
[7] J. Lundkvist, J. Naslund, Gamma-secretase: a complex target for Alzheimer's disease, Curr. Opin. Pharmacol. 7 (2007) 112–118.
[8] S.L. Roberds, J. Anderson, G. Basi, M.J. Bienkowski, L. McConlogue, BACE knockout mice are healthy despite lacking the primary beta secretase activity in brain: implications for Alzheimer's disease therapeutics, Hum. Mol. Genet. 10 (2001) 1317–1324.
[9] S. Patel, L. Vuillard, A. Cleasby, C.W. Murray, J. Yon, Apo and inhibitor complex structures of BACE (β-secretase), J. Mol. Biol. 343 (2004) 407–416.
[10] S. Chakraborty, S. Kumar, S. Basu, Conformational transition in the substrate binding domain of β-secretase exploited by NMA and its implication in inhibitor recognition: BACE1–myricetin a case study, Neurochem. Int. 58 (2011) 914–923.
[11] L. Hong, G. Koelsch, X. Lin, S. Wu, S. Terzyan, A.K. Ghosh, X.C. Zhang, J. Tang, Structure of the protease domain of memapsin 2 (beta-secretase) complexed with inhibitor, Science 290 (2000) 150–153.
[12] A.K. Ghosh, N. Kumaragurubaran, L. Hong, H. Lei, K.A. Hussain, C.-F. Liu, T. Devasamudram, V. Weerasena, R. Turner, G. Koelsch, G. Bilcer, J. Tang, Design, synthesis and X-ray structure of protein–ligand complexes: important insight into selectivity of memapsin 2 (β-secretase) inhibitors, J. Am. Chem. Soc. 128 (2006) 5310–5311.
[13] S. Chakraborty, B. Ramachandran, S. Basu, Encompassing receptor flexibility in virtual screening using ensemble docking-based hybrid QSAR: discovery of novel phytochemicals for BACE1 inhibition, Mol. BioSyst. 10 (2014) 2684–2692.
[14] J. Viklund, K. Kolmodin, G. Nordvall, B.M. Swahn, M. Svensson, Y. Gravenfors, F. Rahm, Creation of novel cores for β-secretase (BACE-1) inhibitors: a multiparameter lead generation strategy, ACS Med. Chem. Lett. 5 (2014) 440–445.
[15] A.A. Gorfe, A. Caflisch, Functional plasticity in the substrate binding site of β-secretase, Structure 13 (2005) 1487–1498.
[16] R.T. Turner, L. Hong, G. Koelsch, A.K. Ghosh, J. Tang, Structural locations and functional roles of new subsites S5, S6, and S7 in memapsin 2 β-secretase, Biochemistry 44 (2005) 105–112.
[17] Y. Xu, M.J. Li, H. Greenblatt, W. Chen, A. Paz, O. Dym, Y. Peleg, T. Chen, X. Shen, J. He, H. Jiang, I. Silman, J.L. Sussman, Flexibility of the flap in the active site of BACE1 as revealed by crystal structures and molecular dynamics simulations, Acta Crystallogr. D Biol. Crystallogr. 68 (2011) 13–25.
[18] L. Hong, J. Tang, Flap position of free memapsin 2 (β-secretase), a model for flap opening in aspartic protease catalysis, Biochemistry 43 (2004) 4689–4695.
[19] H. Shimizu, A. Tosaki, K. Kaneko, T. Hisano, T. Sakurai, N. Nukina, Crystal structure of an active form of BACE1, an enzyme responsible for amyloid β protein production, Mol. Cell. Biol. 28 (2008) 3663–3671.
[20] A. Capell, H. Steiner, M. Willem, H. Kaiser, C. Meyer, J. Walter, S. Lammich, G. Multhaup, C. Haass, Maturation and pro-peptide cleavage of beta-secretase, J. Biol. Chem. 275 (2000) 30849–30854.
[21] R. Ehehalt, P. Keller, C. Haass, C. Thiele, K. Simons, Amyloidogenic processing of the Alzheimer beta-amyloid precursor protein depends on lipid rafts, J. Cell Biol. 160 (2003) 113–123.
[22] X.P. Huang, W.P. Chang, G. Koelsch, R.T. Turner III, F. Lupu, J. Tang, Internalization of exogenously added memapsin 2 (beta-secretase) ectodomain by cells is mediated by amyloid precursor protein, J. Biol. Chem. 279 (2004) 37886–37894.
[23] J. Walter, R. Fluhrer, B. Hartung, M. Willem, C. Kaether, A. Capell, S. Lammich, G. Multhaup, C. Haass, Phosphorylation regulates intracellular trafficking of beta-secretase, J. Biol. Chem. 276 (2001) 14634–14641.
[24] V. Buggia-Pre'vot, C.G. Fernandez, V. Udayar, K.S. Vetrivel, A. Elie, J. Roseman, V.A. Sasse, M. Lefkow, X. Meckler, S. Bhattacharyya, M. George, S. Kar, V.P. Bindokas, A.T. Parent, L. Rajendran, H. Band, R. Vassar, G. Thinakaran, A function for EHD family proteins in unidirectional retrograde dendritic transport of BACE1 and Alzheimer's disease Ab production, Cell Rep. 5 (2013) 1552–1563.
[25] J.M. Sauder, J.W. Arthur, R.L. Dunbrack Jr., Modeling of substrate specificity of the Alzheimer's disease amyloid precursor protein β-secretase, J. Mol. Biol. 300 (2000) 241–248.
[26] B.J. Grant, A.A. Gorfe, J.A. McCammon, Large conformational changes in proteins: signaling and other functions, Curr. Opin. Struct. Biol. 20 (2010) 142–147.
[27] O. Sperandio, L. Mouawad, E. Pinto, O.V. Bruno, D. Perahia, M.A. Miteva, How to choose relevant multiple receptor conformations for virtual screening: a test case of Cdk2 and normal mode analysis, Eur. Biophys. J. 39 (2010) 1365–1372.
[28] B. Hess, C. Kutzner, D.V.D. Spoel, E. Lindahl, GROMACS 4: algorithms for highly efficient, load-balanced, and scalable molecular simulation, J. Chem. Theory Comput. 4 (2008) 435–447.
[29] H.J. Berendsen, D.V.D. Spoel, R.V. Drunen, GROMACS: a message-passing parallel molecular dynamics implementation, Comput. Phys. Commun. 91 (1995) 43–56.
[30] W.L. Jorgensen, T. Rives, Development and testing of the OPLS all-atom force field on conformational energetic and properties of organic liquids, J. Am. Chem. Soc. 110 (1988) 1657–1666.
[31] K. Arnold, L. Bordoli, J. Kopp, T. Schwede, The SWISS-MODEL workspace: a web-based environment for protein structure homology modeling, Bioinformatics 22 (2006) 195–201.
[32] S.R. Comeau, D.W. Gatchell, S. Vajda, C.J. Camacho, ClusPro: an automated docking and discrimination method for the prediction of protein complexes, Bioinformatics 20 (2004) 45–50.
[33] D. Kozakov, R. Brenke, S.R. Comeau, S. Vajda, PIPER: an FFT-based protein docking program with pairwise potentials, Proteins Struct. Funct. Bioinforma. 65 (2006) 392–406.
[34] N. London, B. Raveh, E. Cohen, G. Fathi, O. Schueler-Furman, Rosetta FlexPepDock web server — high resolution modeling of peptide–protein interactions, Nucleic Acids Res. 39 (Suppl. 2) (2011) W249–W253.
[35] B. Hess, H. Bekker, H.J.C. Berendsen, J.G.E.M. Fraaije, LINCS: a linear constraint solver for molecular simulations, J. Comput. Chem. 18 (1997) 1463–1472.
[36] T.E. Cheatham, J.L. Miller, T. Fox, T.A. Darden, P.A. Kollman, Molecular dynamics simulations on solvated biomolecular systems — the Particle Mesh Ewald Method leads to stable trajectories of DNA, RNA, and proteins, J. Am. Chem. Soc. 117 (1995) 4193–4194.
[37] E. Papaleo, P. Mereghetti, P. Fantucci, R. Grandori, L. De Gioia, Free-energy landscape, principal component analysis, and structural clustering to identify representative conformations from molecular dynamics simulations: the myoglobin case, J. Mol. Graph. Model. 27 (2009) 889–899.
[38] W. Im, D. Beglov, B. Roux, Continuum solvation model: computation of electrostatic forces from numerical solutions to the Poisson–Boltzmann equation, Comput. Phys. Commun. 111 (1998) 59–75.
[39] S. Jo, M. Vargyas, J. Vasko-Szedlar, B. Roux, W. Im, PBEQ-solver for online visualization of electrostatic potential of biomolecules, Nucleic Acids Res. 36 (2008) W270–W275.
[40] S. Hayward, H.J.C. Berendsen, Systematic analysis of domain motions in proteins from conformational change; new results on citrate synthase and T4 lysozyme, Proteins Struct. Funct. Genet. 30 (1998) 144–154.
[41] K.G. Tina, R. Bhadra, N. Srinivasan, PIC: protein interactions calculator, Nucleic Acids Res. 35 (2007) W473–W476.